Chemical Science

ROYAL SOCIETY OF CHEMISTRY

EDGE ARTICLE

View Article Online
View Journal

Cite this: DOI: 10.1039/d6sc00984k

All publication charges for this article have been paid for by the Royal Society of Chemistry

Received 4th February 2026
Accepted 6th May 2026

DOI: 10.1039/d6sc00984k

rsc.li/chemical-science

Direct arylation polymerization of electron-rich arenes with polar-group tolerance enabled by ligand-coordination tuning

Xilin Pei,†[abcd] Wei Wu,†[acd] Yanlu Sun,[e] Quan Yang,[acd] Jianan Weng,[acd] Shuhua Zhang,[acd] Zhi Geng[acd] and Bo Zhu *[acd]

Electron-rich arenes are crucial building blocks in conjugated polymers due to their strong electron-donating properties and tunable electronic structures, underpinning diverse applications in organic electronics, biointerfaces, and energy technologies. However, the pronounced π-delocalization of electron-rich arenes can increase the arene distortion and reorganization energy required at the transition state, making efficient C–H activation under typical phosphine conditions challenging, particularly when polar substituents simultaneously compete for Pd coordination. The absence of a comprehensive mechanistic understanding of interactions among ligands, catalysts, arenes, and polar substituents has forced researchers to rely on empirical condition screening, significantly limiting synthetic efficiency and the scope of functional polymers. Using 3,4-ethylenedioxythiophene (EDOT) and its derivatives as representative electron-rich monomers, we demonstrate that the phosphine ligand coordination strength, quantified by electron-donating strength (EDS), critically governs both the C–H activation efficiency and the catalyst's tolerance toward polar groups. Weak-donating ligands facilitate Pd–C formation and disrupt localized π-delocalization, significantly enhancing C–H activation. Conversely, the more donating ligands within the weak-donating series, strengthen Pd-phosphine interaction relative to Pd-polar-group coordination, shifting the coordination balance away from inhibitory polar-group-bound Pd states and thereby mitigating catalyst poisoning. This mechanistic insight provides a predictive framework for rational condition selection in DArP, replacing empirical screening with a design-driven strategy. The resulting protecting-group-free strategy provides scalable access to high-molecular-weight conjugated polymers bearing diverse functionalities, including the notoriously catalyst-deactivating amines, and expands the synthetic toolkit for functional conjugated polymers in organic electronics, biointerfaces, and energy applications.

Introduction

3,4-Ethylenedioxythiophene (EDOT) is a central electron-rich building block for conducting and semiconducting polymers. EDOT-based polymers, especially PEDOT and its derivatives, are widely used in organic electronics, bioelectronics, sensing, and energy-related devices because of their redox stability, electrical conductivity, electrochemical robustness, and mixed ionic–electronic transport.[1–14] Introducing polar substituents such as hydroxyl, carboxyl, or amine groups into EDOT-based polymers is attractive because these groups can improve processability, tune interfacial interactions, modulate charge transfer, and provide chemical handles for further functionalization. However, the protecting-group-free synthesis of high-molecular-weight polar-functionalized EDOT polymers remains difficult because it requires efficient C–H activation of the electron-rich EDOT core while simultaneously managing polar substituents that can affect solubility, alter catalyst coordination, and deactivate transition-metal catalysts.[15,16]

Direct arylation polymerization (DArP) is particularly appealing for EDOT-based polymer synthesis because it forms aryl–aryl bonds directly from arene C–H bonds and aryl halides, avoiding the organometallic monomers required in Stille, Suzuki, and Kumada polymerizations.[17–24] Several DArP protocols have enabled the polymerization of EDOT-type monomers, demonstrating that EDOT arylation is feasible under optimized catalytic conditions.[25–29] Nevertheless, these successes remain

[a]School of Materials Science and Engineering, Shanghai University, Shanghai 200444, China. E-mail: bozhu@shu.edu.cn; titbiam@gmail.com

[b]State Key Laboratory for Modification of Chemical Fibers and Polymer Materials, Innovation Center for Textile Science & Technology, College of Material Science and Engineering, Donghua University, Shanghai 201620, China

[c]Shanghai Engineering Research Center of Organ Repair, Shanghai University, Shanghai 200444, China

[d]Joint International Research Laboratory of Biomaterials and Biotechnology in Organ Repair, Ministry of Education, China

[e]College of Textiles, Donghua University, Shanghai 201620, China

† These authors contributed equally: Xilin Pei, Wei Wu.

largely condition-specific, and a predictive framework for selecting ligands for polar-functionalized EDOT monomers remains lacking. This limitation becomes critical when hydroxyl, carboxyl, or amine groups are introduced, because catalyst performance then depends not only on C–H activation efficiency but also on resistance to nonproductive coordination by polar substituents.

In Pd-catalyzed direct arylation, C–H cleavage commonly proceeds through a concerted metalation–deprotonation (CMD) pathway, in which the Pd center and a coordinated carboxylate, such as pivalate, cooperate to cleave the C–H bond.[30–32] Importantly, CMD is not governed by arene electron density in the manner expected for electrophilic aromatic substitution; both electron-rich and electron-poor arenes can undergo CMD-based activation when the catalyst environment is properly matched to the substrate. Therefore, EDOT-type monomers should not be viewed as intrinsically unreactive. Rather, our calculations suggest that EDOT's pronounced π-delocalization can increase the arene distortion and π-bond reorganization required to reach the CMD transition state.

Moreover, polar substituents introduce an additional, mechanistically distinct complication. Heteroatom-containing groups can serve as directing groups in small-molecule C–H activation, but under DArP conditions, they may instead act as competitive ligands that bind Pd in off-cycle states and suppress catalytic turnover.[33–39] Primary amines are particularly problematic because their strong σ-donating ability and high affinity for Pd(II) can severely deactivate the catalyst. Protecting groups can mask these interactions, but they add synthetic steps and reduce the step-economy advantage of DArP.

Here, we address this challenge through ligand-coordination-tuned DArP using polar-functionalized EDOT derivatives as representative monomers. Across eleven phosphine ligands, combined experimental and computational analyses identify phosphine electron-donating strength (EDS) as a practical descriptor that regulates both CMD-based C–H activation and tolerance toward coordinating polar groups. More weakly donating ligands strengthen Pd(4d)–C(2p) interaction at the CMD intermediate and transition state, promoting Pd–C bond formation and the arene distortion that locally disrupts π-delocalization. More donating ligands, in contrast, strengthen Pd-phosphine coordination relative to Pd-polar-group coordination, shifting the coordination equilibrium away from persistent off-cycle polar-group-bound Pd species (Fig. 1B). Balancing these opposing effects through precise tuning of ligand EDS explains why ligands with moderate-donating strength achieve optimal performance, simultaneously enabling efficient arene activation and DArP and minimizing catalyst deactivation. This mechanistic framework shifts ligand selection in DArP of electron-rich arenes from empirical trial-and-error toward rational and design-driven synthesis. We envision that the resulting ligand-coordination-tuned approach provides a general, sustainable, and predictive strategy for accessing diverse high-molecular-weight conjugated EDOT polymers, significantly expanding synthetic capabilities and advancing materials development in organic electronics, biointerfaces, and energy applications.

Results and discussion

Modulating DArP of EDOT monomers *via* ligand electron-donating strength

We selected eleven monophosphine ligands, including strong-donating alkyl phosphines (**L1–L3**), moderate-donating aryl phosphines (**L4–L6**), and weak-donating aryl phosphines (**L7–L11**), as ligands for the Pd catalyst to activate the C–H bonds of electron-rich EDOT derivatives and polymerize them. We first evaluated their EDS qualitatively by measuring the coupling constants (J_{Rh-P}) in the ^{31}P NMR spectra of their complexes with rhodium ([RhCl(CO)(Ln)$_2$]) (Fig. 2B), as a weaker coordination strength typically leads to a higher J_{Rh-P}.[40] However, for **L6**, its methoxy substituent competes with the phosphorus atom to interact with rhodium, reducing the phosphorus's contribution and causing J_{Rh-P} to deviate. In addition to electronic properties, the steric profile of the ligands (particularly those with aryl *ortho*-substituents, *i.e.*, **L5**, **L6**, **L7**, and **L11**) also influences their coordination behavior.

The functionalized EDOT-based polymers were synthesized *via* a general palladium-catalyzed cross-coupling polymerization. The degree of polymerization (DP) of the hydroxyl-functionalized EDOT (EDOT-OH) and EDOT copolymers (**PEE-OH**), synthesized at 120 °C for 1 h (**L4–L11**), was determined using solution-state ^1H NMR spectroscopy, as GPC measurements did not yield reliable results, likely due to column adsorption caused by hydrazine, which was used to reduce the polymers and improve their solubility. DPs increased dramatically with the J_{Rh-P} values of the ligands **L4–L11** (Fig. 2C and D). Specifically, weak-donating ligands were associated with significantly higher polymer yields and degrees of polymerization than the more strongly donating ligands. Their UV-Vis spectra confirmed this trend, demonstrating a general red shift in λ_{max} with higher J_{Rh-P} values (Fig. 2E), consistent with the extended conjugation typical of higher molecular weights in conjugated polymers. The yields for those reactions with weak-donating ligands were also higher. No products were available with the strong-donating alkyl-phosphine ligands (**L1–L3**).

The DP value of the polymer synthesized with the **L11** ligand was 30, with an 88% yield. To verify this unique ligand effect with a different aryl bromide, we replaced 2,5-dibromo-3,4-ethylenedioxythiophene with 1,4-dibromobenzene and synthesized its copolymer with EDOT-OH (**PPE-OH**) by reacting them at 120 °C for 1 h. The weak-donating ligands again produced polymers with much higher molecular weights and higher yields (Fig. 2F). The DP value of **PPE-OH**, which differed from that of **PEE-OH**, exhibited exponential growth as the J_{Rh-P} value increased (Fig. 2G). The UV results further verified this trend (Fig. 2H). This result indicated that the **PPE-OH** growth was more sensitive to the ligand EDS than the **PEE-OH** growth. We attribute this enhanced sensitivity to the electron deficiency and weak coordinating ability of benzene relative to EDOT, which mimics the behavior of weak-donating ligands. The DP reached an impressive value of 972, with a 92% yield, when using **L11**. Additionally, no significant side-group interference was detected during the polymerization of **PEE-OH** and **PPE-OH**.

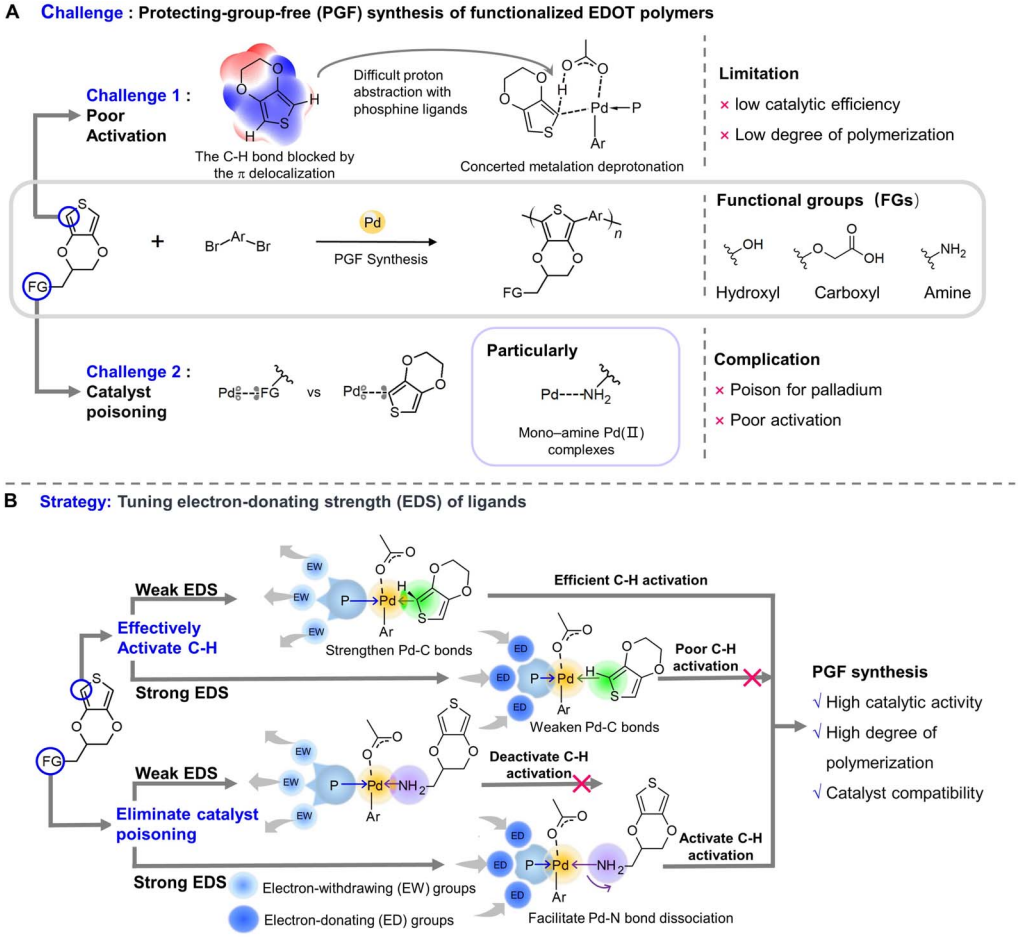

Fig. 1 Ligand-coordination-tuned direct arylation polymerization for synthesizing functionalized EDOT polymers. (A) The two challenges for the synthesis of functionalized EDOT polymers by palladium-catalyzed direct arylation polymerization are poor activation of electron-rich EDOT derivatives and catalyst poisoning of side polar groups. (B) Tuning the electron-donating strength of phosphine ligands facilitates the concerted metalation–deprotonation of EDOTs and direct arylation polymerization of functionalized EDOT polymers.

Furthermore, **PPE-OH** was polymerized *via* DArP under ligand-less conditions (a DP of 108) and with azacyclo-auxiliary ligands (*e.g.*, pyridine, resulting in a DP of 9), both of which demonstrated substantially lower polymerization efficiency compared to using **L11**. This result suggests that tuning the ligand EDS, particularly when using phosphine-based ligands, plays a critical role in enhancing polymerization performance.

To further evaluate the **L11** conditions, we examined **PEE-OH** at extended reaction time and **PPE-OH** at shortened reaction time. The DP of **PEE-OH** increased significantly to 86, with a 91% yield after extending the reaction time to 24 h (Table S3). **PPE-OH** still achieved a high DP value of 176, with an 83% yield after reducing the reaction time to 30 min (Table S4). These results demonstrate, respectively, the durability and reactivity of the **L11**-based system. Additionally, the DPs of **PEE-OH** (86) after 24 h and **PPE-OH** (972) after 1 h under **L11** conditions are significantly higher than those obtained under ligand-free conditions (77 and 108, respectively), despite identical reaction parameters (Tables S3 and S4).

To benchmark our **L11** system against efficient DArP conditions reported for EDOT-type monomers, we performed comparative experiments using literature-adapted $Pd_2(dba)_3$/*o*-methoxytriphenylphosphine (**L6**)/PivOH/toluene conditions.[26,41–43] For **PEE-OH**, the benchmark system using 2 mol% $Pd_2(dba)_3$, 4 mol% **L6**, Cs_2CO_3, and PivOH in toluene at 110 °C gave DPs of 23 and 29 after 1 and 48 h, with yields of 31% and 32%, respectively (Table S3), lower than the DP of 86 obtained with **L11**. For **PPE-OH**, the same benchmark conditions gave DPs of 14 and 17 after 1 and 48 h, respectively (Table S4), far below the DP of 972 achieved with **L11**.

A higher-loading variant of the **L6**/toluene system using 10 mol% $Pd_2(dba)_3$, 20 mol% **L6**, and KPivO led to extensive toluene-derived end-capping or solvent incorporation for both **PEE-OH** and **PPE-OH**, making reliable DP determination difficult. In contrast, the **L11**/$Pd(OAc)_2$/DMAc/KPivO system showed no detectable solvent- or ligand-derived incorporation and afforded higher-DP polymers with cleaner end-group behavior.

We then used carboxyl-functionalized EDOT (EDOT-COOH) as an arylation substrate instead to synthesize copolymers with EDOT/benzene (**PEE-COOH**/**PPE-COOH**) and found that **L5**, **L6**, **L7**, and **L11** gave no products (Fig. 3A and B). A common feature of these ligands was their *ortho* substituents on their

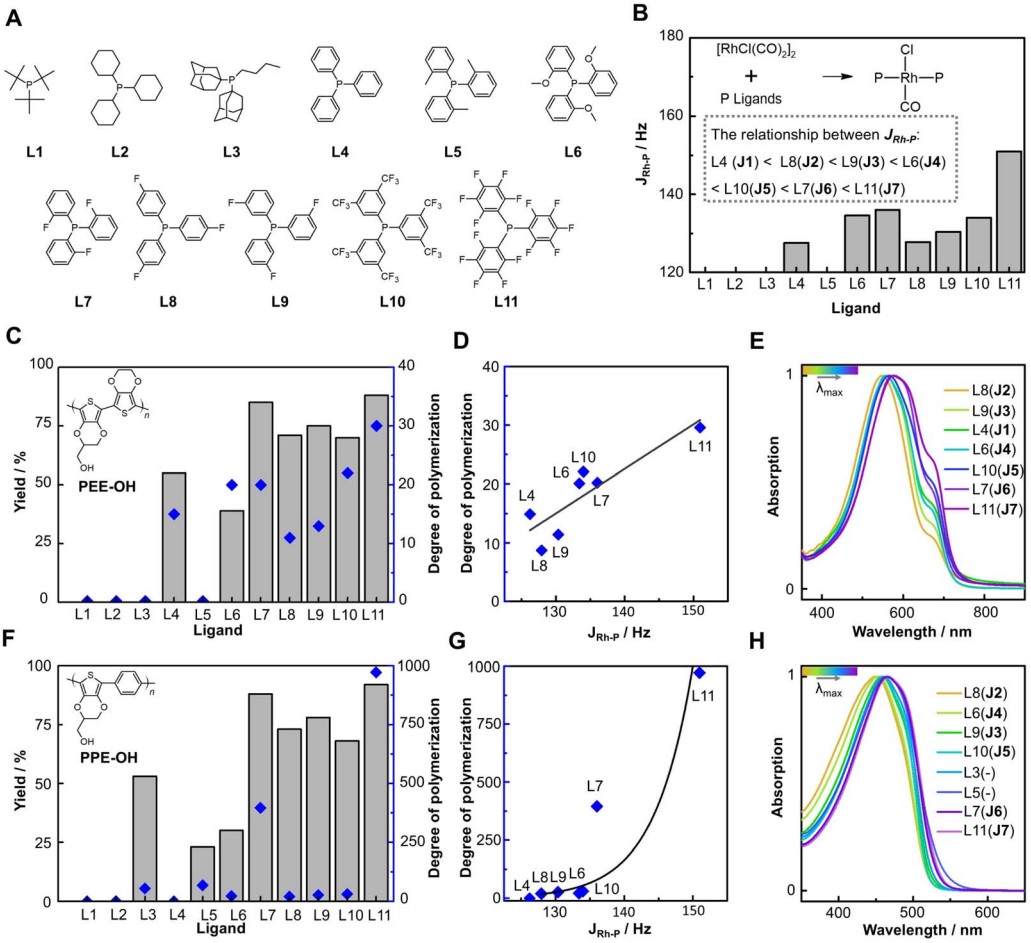

Fig. 2 Effect of ligands' electron-donating strength (EDS) on the direct arylation polymerization of hydroxyl functionalized EDOT (EDOT-OH). (A) The phosphine ligands used in this study. (B) EDS values of aryl-phosphine ligands evaluated by the coupling constants (J_{Rh-P}) of [RhCl(CO)(Ln)$_2$]s in their ^{31}P NMR spectra. (C) The degrees of polymerization (DPs) and the yields of the copolymers of EDOT-OH with EDOT (**PEE-OH**s) synthesized using the phosphine ligands shown in (A). **PEE-OH**s were synthesized on a 0.25 mmol scale using EDOT-OH (1 eq.), dibromo-EDOT (1 eq.), Pd(OAc)$_2$ (10 mol%), phosphine ligand (20 mol%), and KPivO (2 eq.) in DMAc (0.125 M) at 120 °C for 1 h. (D) The plot of the **PEE-OH** DPs as a function of J_{Rh-P}. (E) The UV spectra of **PEE-OH**s in DMSO/$N_2H_4{\cdot}H_2O$ (85%) (v/v = 100 : 1). (F) The DPs and the yields for the copolymers of EDOT-OH with benzene (**PPE-OH**s) synthesized using the phosphine ligands shown in 2A. **PPE-OH**s were synthesized on a 0.25 mmol scale using EDOT-OH (1 eq.), dibromobenzene (1 eq.), Pd(OAc)$_2$ (10 mol%), phosphine ligand (20 mol%), and KPivO (2 eq.) in DMAc (0.125 M) at 120 °C for 1 h. (G) The plot of the **PPE-OH** DPs as a function of J_{Rh-P}. (H) The UV spectra of **PPE-OH**s in DMSO/$N_2H_4{\cdot}H_2O$.

phenyl rings, which provided significant steric hindrance to prevent EDOT-COOH from approaching. As evaluated by the Tolman cone angles,[44,45] the *ortho*-substituted phosphine ligands with cone angles ≥ 135°, *i.e.*, **L5**, **L6**, **L7**, and **L11**, gave no **PEE-COOH** or **PPE-COOH** product, while **L10**, with a slightly smaller cone angle of 134°, retained partial activity (Fig. 3C). We considered that under basic conditions, EDOT-COOH would complex with Pd through the carboxylate and ester oxygen to form a stable five-membered chelate (Fig. 3D) and thus amplify the steric effect of the ligands on the reactivities of intermediates.[36] **PEE-COOH** and **PPE-COOH** only dissolved in aqueous hydrazine. However, it is difficult to measure their molecular weights from the ^{1}H NMR spectra of their aqueous solutions, as the diagnostic α-proton resonance of the terminal EDOT unit cannot be observed, plausibly because of H/D exchange with the deuterated solvent. The similar UV absorption maxima of **PEE-COOH**s suggest comparable conjugation lengths under the tested conditions, likely limited by poor solubility in DMAc. In contrast, the red-shifted absorption of **PPE-COOH**s with decreasing ligand EDS qualitatively indicates extended conjugation and more efficient EDOT-COOH arylation under selected ligand conditions, consistent with the weak-ligand-enhanced activation trend discussed above (Fig. 3E and F).

Activating the primary amine-functionalized arene remains a considerable challenge, as it competes with the arene substrates for tight coordination with Pd, typically deactivating the Pd catalyst. Consistent with this expectation, the copolymer of amine-functionalized EDOT (EDOT-NH_2) with EDOT (**PEE-NH_2**) gave low DPs and yields under the conditions optimized for **PEE-OH** (**L7** and **L11**), even when the reaction time was extended to 6 h (Fig. 3G and I). The small molecule model also confirmed that the **L7** and **L11** conditions are inactive in arylating EDOT-NH_2 with 2-bromo-5-methylthiophene and bromobenzene (Fig. S2 and S3). As ligand EDS increased,

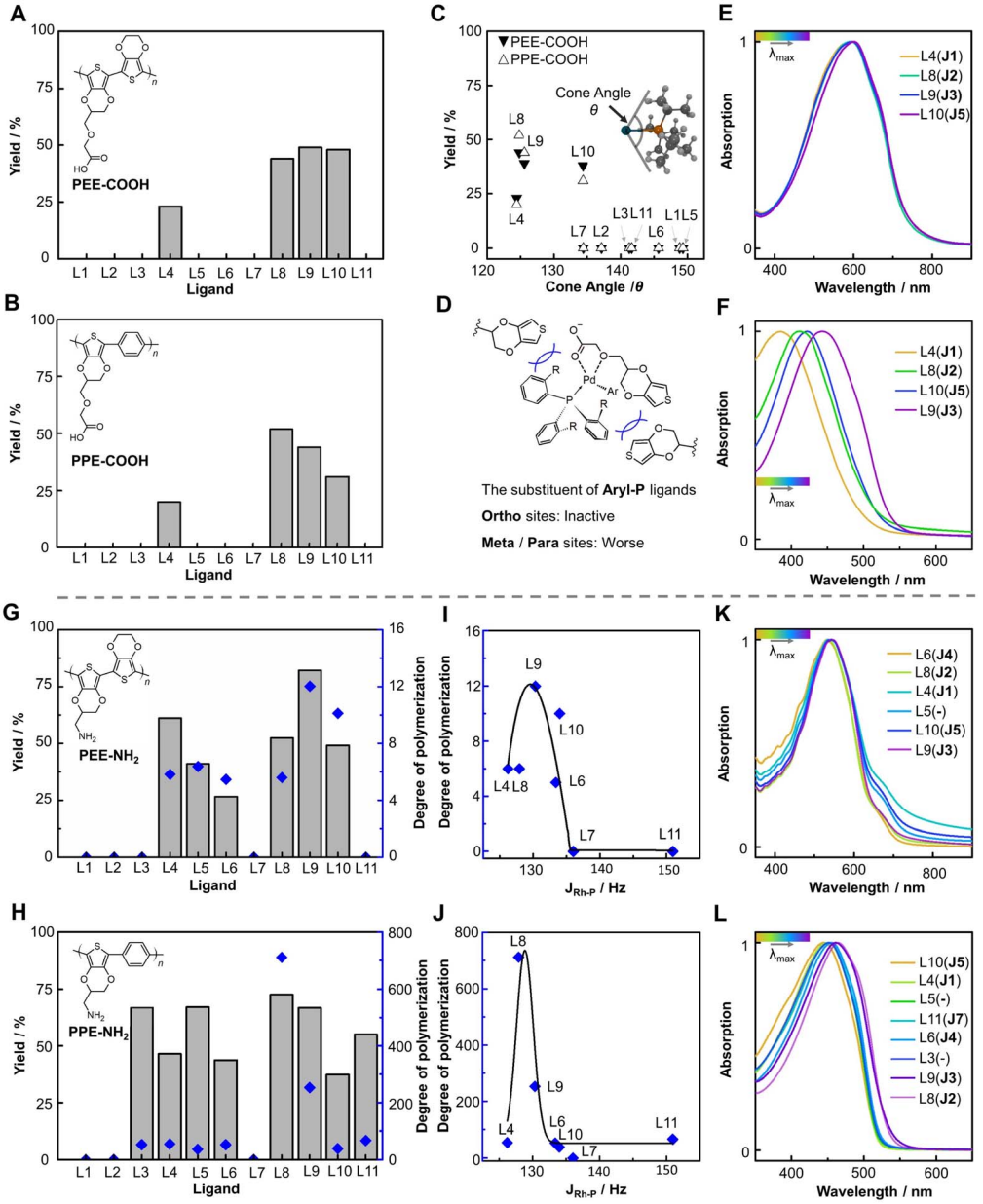

Fig. 3 Compatibility of carboxyl and amine groups with palladium catalyst in direct arylation polymerization. (A and B) The yield for (A) the copolymers of EDOT-COOH with EDOT (**PEE-COOH**s) and (B) those of EDOT-COOH with benzene (**PPE-COOH**s) using phosphine ligands listed in Fig. 2A. **PEE-COOH**s and **PPE-COOH**s were synthesized on a 0.25 mmol scale using EDOT-COOH (1 eq.), arene dibromide (1 eq.), $Pd(OAc)_2$ (10 mol%), phosphine ligand (20 mol%) and KPivO (2 eq.) in DMAc (0.125 M) at 120 °C for 1 h. (C) The plot of the yields of **PEE-COOH**s and **PPE-COOH**s as a function of the cone angle of phosphine ligands. The embedded graph illustrates the Tolman cone-angle representation for **L1**, with the M–P distance fixed at 2.28 Å. The geometry optimization of phosphine ligands was done using M06L/6-31G(d), and the Tolman cone angles were calculated by Solid-G software. (D) Schematic illustration of how *ortho*-substituents on the aryl-phosphine ligands sterically block approach of the EDOT-COOH substrate to the Pd center. (E and F) The UV spectra of the synthesized (E) **PEE-COOH**s and (F) **PPE-COOH**s in $N_2H_4{\cdot}H_2O$ (85%) solutions. (G and H) The DPs and the yields for (G) the copolymer of EDOT-NH_2 with EDOT (**PEE-NH$_2$**) and (H) that of EDOT-NH_2 with benzene (**PPE-NH$_2$**) using phosphine ligands listed in Fig. 2A. **PEE-NH$_2$** and **PPE-NH$_2$**s were synthesized on a 0.25 mmol scale using EDOT-NH_2 (1 eq.), arene dibromide (1 eq.), $Pd(OAc)_2$ (10 mol%), phosphine ligand (20 mol%) and KPivO (2 eq.) in DMAc (0.125 M) at 120 °C for 6 h. (I and J) The plots of the (I) **PEE-NH$_2$** DPs and the (J) **PPE-NH$_2$** DPs as a function of J_{Rh-P}. (K and L) The UV spectra of the synthesized (K) **PEE-NH$_2$** and (L) **PPE-NH$_2$** in DMSO/$N_2H_4{\cdot}H_2O$ (85%) (v/v = 100 : 1).

however, the DPs of **PEE-NH$_2$** rose sharply, implying partial or complete release of primary amine groups from the Pd catalyst. After the DPs and yields reached their maximum at **L9**, they decreased with further increases in ligand EDS. A similar phenomenon was also observed in synthesizing the copolymer of EDOT-NH_2 and benzene (**PPE-NH$_2$**) (Fig. 3H). A striking DP (711) was achieved for **PPE-NH$_2$** synthesized with **L8**, with a yield of 73%. Furthermore, this unique dependence of molecular

weight on EDS was further confirmed by the results of the 1 h and 3 h reactions (Tables S7 and S8).

To determine whether this volcano-shaped trend reflects intrinsic arylation chemistry rather than polymerization-specific effects, we conducted model reactions of EDOT-NH_2 with 2-bromo-5-methylthiophene or bromobenzene under analogous conditions. These reactions reproduced the same ligand dependence, with **L7** and **L11** showing little activity, **L8** and **L9** giving the highest EDOT-NH_2 consumption, and more donating ligands such as **L4** showing reduced activity (Fig. S5). Because these model reactions do not involve chain growth, the trend cannot be mainly attributed to chain-extension kinetics, solubility changes, or accumulation of amine-containing repeat units.

We propose that amine coordination is also strongly influenced by the ligand's EDS but in a manner opposite to the DArP activity of electron-rich arenes, necessitating a trade-off between the two processes to facilitate efficient polymerization. Accordingly, the highest DPs for both the EDOT-NH_2 copolymers were achieved using an optimized ligand with a medium EDS (Fig. 3I and J). These results highlight the importance of balancing between the amine coordination and the DArP activity of electron-rich arenes by tuning the ligand's EDS to overcome amine-induced catalyst poisoning. Matched-cone-angle comparisons (Tables S7 and S8) further show that the ligand effect cannot be explained by steric effects alone, as **L8** greatly outperforms **L4** in **PPE-NH_2**, despite nearly identical cone angles, and **L9** similarly outperforms **L4** in **PEE-NH_2**. This electronic-effect explanation is further supported by the ligand-free benchmark, which gave moderate activity for **PEE-OH** and **PPE-OH** polymerization but only low DPs (3 and 20) and yields (23% and 41%) for **PEE-NH_2** and **PPE-NH_2**, respectively (Tables S7 and S8).

Weak ligand coordination promotes deprotonation

To uncover the unique effect of ligand EDS on the DArP activity of electron-rich EDOT substrates, we employed DFT to compute Gibbs free-energy profiles for the C–H activation step across the **L4–L11** ligand series, focusing on the concerted metalation–deprotonation (CMD) pathway as the operative mechanism. A typical CMD process for the C–H activation of EDOT alpha carbon, where two intermediates (**Pre-TS** and **Post-TS**) occur before and after the transition state (**TS**),[46] is shown in Fig. 4A. The ΔG values for both direct arylations of EDOT with EDOT and benzene reached the minimum when the weakest-donating ligand (**L11**) was used (Tables S10 and S12). These results strongly corroborate the experimental findings, underscoring the pivotal role of the ligand EDS in facilitating the C–H activation of electron-rich EDOT derivatives.

To gain deeper insight into the CMD processes, we performed natural bond orbital (NBO) analysis on the EDOT–EDOT coupling at both the **Pre-TS** and **TS** stages. The more weakly donating ligands (those with higher J_{Rh-P} values) corresponded to lower Wiberg bond orders (WBOs) for the Pd–P bond at **Pre-TS**. This weakening of the Pd–P interaction coincided with a strengthened Pd–C bond, directly supporting the notion that weaker ligands promote stronger Pd–C bonding (Fig. 4B). A similar trend was observed at the **TS** stage, where both Pd–C and Pd–P WBOs showed a consistent dependence on ligand EDS. Consistent results were also obtained from the NBO analysis of EDOT-benzene coupling, further reinforcing the observed trends (Fig. 4C). We also conducted NAO analyses to decompose the Pd–P and Pd–C WBOs,[47,48] and found that the Pd–P WBO primarily arises from hybridization between the Pd 4d and P 3p orbitals, while the Pd–C WBO is mainly due to hybridization between the Pd 4d and C 2p orbitals. Analysis of their dependences on ligand electron-donating strength (EDS) revealed that decreasing the ligand EDS weakens Pd(4d)–P(3p) hybridization while strengthening Pd(4d)–C(2p) hybridization (Fig. 4D). A comparable trend was observed in the NAO analysis of the coupling between EDOT and benzene substrates (Fig. 4E). All the above findings indicate that reducing ligand EDS promotes Pd–C bond formation by attenuating the Pd–P interaction.

The EDOT distortion energies at the **Pre-TS** for both the EDOT–EDOT and EDOT-benzene couplings are directly proportional to the corresponding Pd–Cα WBOs (Fig. 4F and G), consistent with the observation that both the distortion energies (Fig. S6) and Pd–Cα WBOs (Fig. 4B and C) at the **Pre-TS** exhibit linear correlations with the ligand EDS. This key finding supports the conclusion that stronger Pd–C bonds, resulting from weakened Pd–P interactions, lead to more pronounced EDOT distortion. We further found that this characteristic EDOT distortion at the **Pre-TS** with the weak-donating ligand (**L11**) directly coincides with a significant reduction in localized π-delocalization near Cα, as evidenced by comparisons between EDOT and **Pre-TS** EDOT in the second and fourth highest occupied molecular orbitals (HOMO−1 and HOMO−3) (Fig. 4H and Tables S27, S28). To better understand this phenomenon, we analyzed the correlation between the contribution of Cα(2pz)–Cβ(2pz) orbital hybridization to π-delocalization in the pre-transition state (**Pre-TS**) and the Pd–Cα WBOs, revealing a clear inverse linear relationship (Fig. 4I and J).

Based on these results, we propose that decreasing ligand EDS attenuates Pd(4d)–P(3p) hybridization and allows greater Pd(4d)–C(2p) interaction between the Pd(II) intermediate and the electron-rich EDOT Cα carbon, thereby strengthening Pd–C bond formation during CMD. This interaction distorts the C–H bond and diminishes the adjacent π-delocalization, in turn facilitating proton shuttling from EDOT substrates to the carboxylates. The same EDS principle also rationalizes the inactivity of the strong-donating alkyl phosphines **L1–L3** in the EDOT-rich PEE series, where insufficient activation of the EDOT C–H bond becomes the dominant limitation. This mechanistic insight provides predictive guidance for rational ligand design to achieve high molecular weight EDOT polymers, offering greater flexibility in addressing compatibility challenges associated with polar side groups, as discussed below.

Mitigating catalyst poisoning of polar groups

Heteroatoms bearing lone electron pairs can compete with the arene substrate for coordination at Pd, lowering reactivity and deactivating the catalyst. No catalyst poisoning was observed for

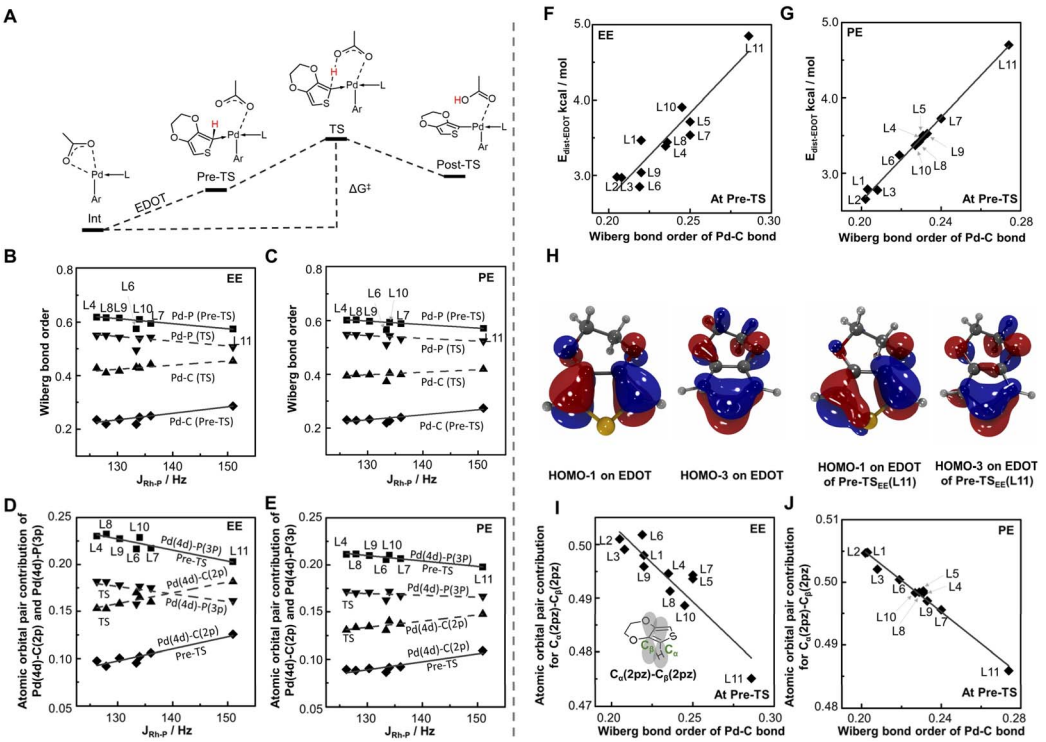

Fig. 4 Weak ligand coordination facilitates deprotonation. (A) The typical concerted metalation–deprotonation (CMD) pathway for EDOT activation, where a prior intermediate (**Pre-TS**) occurs ahead of the transition state (**TS**). (B and C) The plots of the Wiberg bond orders (WBOs) of the Pd–C and Pd–P bonds as a function of J_{Rh-P} for the **Pre-TS** and **TS** of coupling between (B) EDOT/(C) benzene (oxidative addition substrate) and EDOT (arylation substrate). The solid lines represent WBOs at **Pre-TS**; the dotted lines represent those at **TS**. EE/PE indicates the CMD processes involving EDOT/benzene (oxidative addition substrate) and EDOT (arylation substrate). (D and E) The plot of the atomic orbital pair contribution of Pd(4d)–C(2p) to the Pd–C WBO and that of Pd(4d)–P(3p) to the Pd–P WBO as a function of J_{Rh-P} for the **Pre-TS** and **TS** of the coupling between (D) EDOT/(E) benzene (oxidative addition substrate) and EDOT (arylation substrate). The solid lines represent the WBO contributions of the atomic orbital pair at **Pre-TS**; the dotted lines represent those at **TS**. Data for **L6** were excluded from the linear JRh-P fit, as J_{Rh-P} failed to evaluate the **L6** EDS due to the competitive interaction of its methoxy substituent. (F and G) The plots of the EDOT distortion energies as a function of the WBOs for the **Pre-TS** of the coupling between (F) EDOT/(G) benzene (oxidative addition substrate) and EDOT (arylation substrate). (H) The comparison between EDOT and **Pre-TS** EDOT in the second and fourth highest occupied molecular orbitals (HOMO-1 and HOMO-3). (I and J) The plots of the atomic orbital pair contribution of $C_a(2pz)$–$C_b(2pz)$ to the C_α–C_β WBO as a function of J_{Rh-P} for the **Pre-TS** and **TS** of the reaction between (I) EDOT/(J) benzene (oxidative addition substrate) and EDOT (arylation substrate).

the EDOT-OH polymerization, consistent with the weakly coordinating nature of the hydroxyl group (Fig. 5A). In contrast, polymerization of EDOT-COOH was completely suppressed when *ortho*-substituted aryl-phosphine ligands were used (Fig. 3A and B). This result was attributed to the enhanced steric sensitivity of the Pd(II) catalyst once the five-membered carboxylate chelate has formed by the complexation of EDOT-COOH with Pd under basic conditions (Fig. 5B). However, weak-donating ligands of reduced steric profile (*e.g.*, **L9**) can alleviate the geometric constraint imposed by the five-membered chelate, allowing productive Pd–Cα bond formation. In this regime, the Pd-bound EDOT-COOH does not need to dissociate; instead, its carboxylate functions as the proton-shuttle ligand for CMD.

Not surprisingly, EDOT-NH_2 exhibited the strongest catalyst poisoning due to its robust coordination with Pd, forming a stable mono-amine Pd(II) complex (Fig. 5C). This complexation substantially suppressed catalytic activity, resulting in poor yields and low molecular weights for the copolymers of EDOT-NH_2 with EDOT or benzene substrates when synthesized under conditions (**L7** and **L11**) optimized for the EDOT-OH copolymer (Fig. 3G and H). This issue was mitigated by **L8** and **L9**, the more donating members of the weak-donating ligand class, which strengthen Pd-phosphine interaction relative to the most weakly donating ligands **L7** and **L11**, while retaining sufficient weak-donating character to support CMD-based EDOT activation (Fig. 3I and J).

We hypothesized that ligands with relatively stronger donating character within the productive series, *i.e.*, higher EDS than **L7** and **L11**, would promote dissociation of the Pd-amine bond by enhancing the competing Pd-phosphine interaction. To verify this, we performed NBO analyses on mono-amine Pd(II) complexes. The NBO analysis of the mono-amine Pd(II) complexes shows that, as ligand EDS increases, the Pd-phosphine Wiberg bond order rises while the Pd-amine WBO falls in parallel, with the two trends strongly negatively correlated for both EDOT–EDOT and EDOT-benzene couplings (Fig. 5D–G). This coordination-sphere redistribution shifts the catalyst away from persistent Pd-amine-bound off-cycle states.

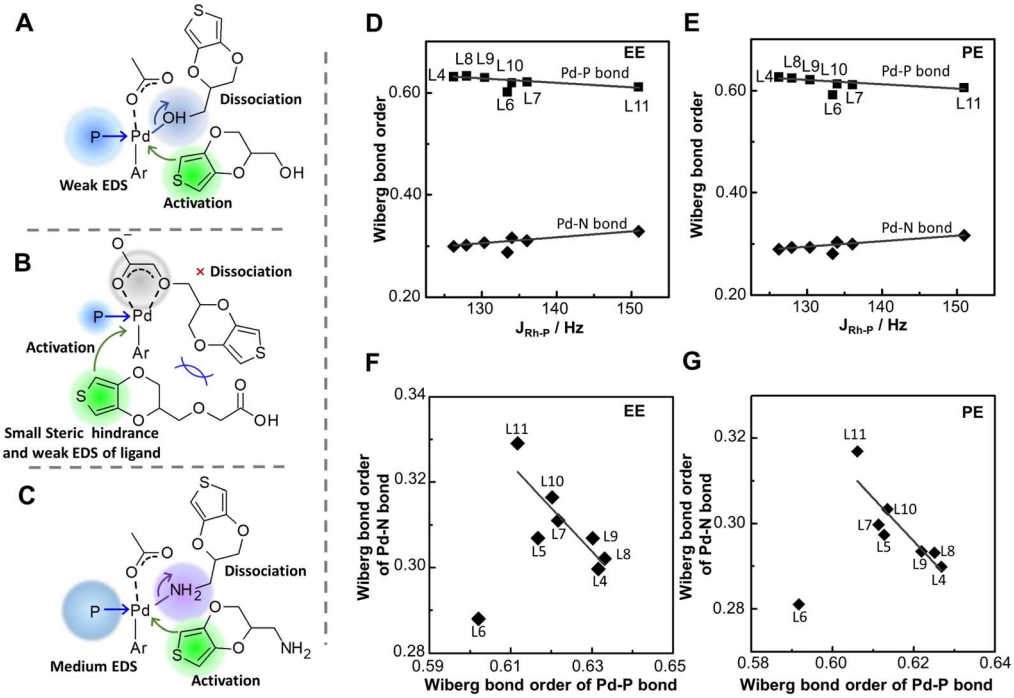

Fig. 5 Tuning ligand properties to achieve compatibility with polar side groups. (A–C) The schematic presentations indicate (A) weak ligand coordination facilitates the C–H arylation of electron-rich EDOT-OH through strengthening the Pd–C bond and promoting deprotonation without the competitive coordination effect from hydroxyl groups due to their weak electron-donating strength (EDS), (B) a combination of weak ligand coordination and small ligand steric hindrance is necessary to activate EDOT-COOH due to the strong electrostatic association of COO^- with palladium, and (C) a phosphine ligand with medium coordination can foster the dissociation of the mono-amine Pd(II) complex and subsequently deprotonation, thus effectively activating EDOT-NH_2. (D and E) The plots for the Pd–N and Pd–P WBOs as a function of J_{Rh-P} for the mono-amine Pd(II) complexes involving (D) EDOT/(E) benzene (oxidative addition substrate) and EDOT-NH_2 (arylation substrate). The descriptions of EE and PE have been provided in Fig. 4B and C. (F and G) The plot of the Pd–N WBO as a function of the Pd–P WBO for the mono-amine Pd(II) complexes involving (F) EDOT/(G) benzene (oxidative addition substrate) and EDOT-NH_2 (arylation substrate). The geometry of mono-amine Pd(II) complexes was optimized using M06L/6-31G(d) and SDD on Pd. The data of **L6** was excluded from being used to fit the linear J_{Rh-P} dependence, as J_{Rh-P} failed to evaluate the **L6** EDS due to the competitive interaction of its methoxy substituent.

Therefore, ligand EDS not only tunes the electronic environment of the Pd center but also governs the suppression of catalyst poisoning by polar functional groups such as amines. By promoting selective dissociation of inhibitory ligands through competitive coordination, the moderately donating ligands within the weak-donating class (**L8** and **L9**) restore the catalytic competence of Pd(II) and enable efficient polymerization. This mechanistic insight is particularly significant for expanding the substrate scope of direct arylation polymerization (DArP) to include functionalized arenes, thus providing a foundation for rational design of conjugated polymers with diverse polar side chains and tailored properties.

Conclusions

In this study, we systematically elucidated, through experimental and computational investigations, how phosphine ligands interact with electron-rich EDOT derivatives and diverse polar side groups through coordination to Pd. We further showed how the electronic nature of these ligands dictates both arene activation and catalyst deactivation in DArP. By parameterizing ligand coordination strength in terms of EDS, we show that more weakly donating phosphines enhance Pd–C bond formation and attenuate local π-delocalization, thereby promoting C–H activation. However, weaker ligand donation also makes the Pd catalyst more susceptible to coordination by polar groups, which can lead to catalyst deactivation. Further analyses show that catalyst poisoning from strongly coordinating side groups, such as amines, can be effectively mitigated by employing the moderately donating ligands within the weak-donating class. These ligands redistribute the Pd coordination sphere toward stronger Pd-phosphine interaction relative to Pd-amine coordination, helping mitigate amine-induced catalyst poisoning and restore catalytic turnover. Striking this optimal balance through precise tuning of ligand EDS proved essential for overcoming the dual challenges of activating electron-rich arenes and suppressing deactivation caused by polar functionalities. Finally, this ligand-coordination-tuned strategy enables the synthesis of high-molecular-weight functionalized conjugated polymers with excellent tolerance to hydroxyl and amine groups, as well as moderate, ligand-dependent compatibility with carboxylic acid functionalities that is sensitive to both steric and electronic ligand effects. This mechanistic clarification of how ligand electronic properties govern both DArP reactivity and catalyst stability establishes a predictive framework for rational ligand selection, transforming ligand design

from empirical trial-and-error into a design-driven strategy. These findings advance the mechanistic understanding of DArP for electron-rich arenes and provide a versatile platform for synthesizing functional conjugated polymers with tailored side groups for organic electronics, biointerfaces, and energy applications.

Experimental

Polymer synthesis *via* DArP

The monomers, including 2,5-dibromo-3,4-ethylenedioxythiophene (DBEDOT), hydroxyl-functionalized EDOT (EDOT-OH), carboxyl-functionalized EDOT (EDOT-COOH), and amine-functionalized EDOT (EDOT-NH_2), were synthesized according to previously reported procedures.[49–51] For polymer synthesis, a general method was employed: in a glovebox, a Schlenk tube was charged with functionalized EDOT monomer (1 equiv.), arene dibromide (1 equiv.), palladium acetate (10 mol%), potassium pivalate (2 equiv.), phosphine ligand (20 mol%), and DMAc (0.125 M monomer) at a 0.25 mmol scale, along with a magnetic stir bar. The mixture was heated in an oil bath at the specified temperature with vigorous stirring for a specified time, then cooled to ambient temperature. Full polymerization details are available in the SI.

Calculation methods

All quantum chemical calculations were performed using Gaussian 09.[52] Density functional theory (DFT) at the M06L level[53] was employed: geometry optimizations and frequency analyses were performed using the SDD basis set for Pd and 6-31G(d) for all other atoms. Single-point energy calculations were then conducted with SDD for Pd and 6-311++G(d,p) for the remaining atoms. Gibbs free energy corrections were obtained by combining these single-point energies with thermal corrections from the frequency calculations, and solvation effects were included using the PCM model with DMAc as solvent to describe the concerted metalation–deprotonation process. Transition states were verified by intrinsic reaction coordinate (IRC) calculations. Electrostatic potential (ESP) mapping, Tolman cone angle estimation,[54] frontier orbital visualization, and Wiberg bond order evaluation based on natural bond orbital (NBO) and natural atomic orbital (NAO) were further carried out.[55] Full computational details are provided in the SI.

Author contributions

B. Z. and X. P. initiated the project and designed the experiments. X. P., W. W., Q. Y. synthesized the monomers and polymers and characterized these materials. X. P., S. Y., J. W. characterized these materials. X. P., B. Z., conducted the computations and mechanistic analysis. X. P., B. Z. wrote the initial draft. B. Z., X. P., S. Z., and Z. G. revised the manuscript. B. Z. supervised the work.

Conflicts of interest

The authors declare no competing interests.

Data availability

The data supporting this study's findings are available from the corresponding author upon reasonable request.

Supplementary information (SI): general methods, experimental procedures, NMR spectra, and calculational details. See DOI: https://doi.org/10.1039/d6sc00984k.

Acknowledgements

We gratefully acknowledge the High Performance Computing Center of Shanghai University and the Shanghai Engineering Research Center of Intelligent Computing System for providing computational resources and support. B. Z. acknowledges the financial support from the NSFC (22175111, 21474014). Z. G. acknowledges the financial support from the NSFC (21704013).

References

1 T. Someya, Z. Bao and G. G. Malliaras, *Nature*, 2016, **540**, 379–385.
2 Z. Zhang, W. Wang, Y. Jiang, Y. X. Wang, Y. Wu, J. C. Lai, S. Niu, C. Xu, C. C. Shih, C. Wang, H. Yan, L. Galuska, N. Prine, H. C. Wu, D. Zhong, G. Chen, N. Matsuhisa, Y. Zheng, Z. Yu, Y. Wang, R. Dauskardt, X. Gu, J. B. Tok and Z. Bao, *Nature*, 2022, **603**, 624–630.
3 A. J. Gillett, A. Privitera, R. Dilmurat, A. Karki, D. Qian, A. Pershin, G. Londi, W. K. Myers, J. Lee, J. Yuan, S.-J. Ko, M. K. Riede, F. Gao, G. C. Bazan, A. Rao, T.-Q. Nguyen, D. Beljonne and R. H. Friend, *Nature*, 2021, **597**, 666–671.
4 Y. Wang, C. Zhu, R. Pfattner, H. Yan, L. Jin, S. Chen, F. Molina-Lopez, F. Lissel, J. Liu, N. I. Rabiah, Z. Chen, J. W. Chung, C. Linder, M. F. Toney, B. Murmann and Z. Bao, *Sci. Adv.*, 2017, **3**, e1602076.
5 Y. Jiang, Z. Zhang, Y.-X. Wang, D. Li, C.-T. Coen, E. Hwanun, G. Chen, H.-C. Wu, D. Zhong and S. Niu, *Science*, 2022, **375**, 1411–1417.
6 B. Zhu, S. C. Luo, H. Zhao, H. A. Lin, J. Sekine, A. Nakao, C. Chen, Y. Yamashita and H. H. Yu, *Nat. Commun.*, 2014, **5**, 4523.
7 T. J. Quill, G. LeCroy, D. M. Halat, R. Sheelamanthula, A. Marks, L. S. Grundy, I. McCulloch, J. A. Reimer, N. P. Balsara, A. Giovannitti, A. Salleo and C. J. Takacs, *Nat. Mater.*, 2023, **22**, 362–368.
8 A. Elschner, k. Stephan, W. Lovenich, U. Merker and K. KReuter, *PEDOT: Principles and Applications of an Intrinsically Conductive Polymer*, Wiley, 2010.
9 H. Dong, E. Zheng, Z. Niu, X. Zhang, Y.-Y. Lin, P. Jain and Q. Yu, *ACS Appl. Mater. Interfaces*, 2020, **12**, 17571–17582.
10 H. Yano, K. Kudo, K. Marumo and H. Okuzaki, *Sci. Adv.*, 2019, **5**, eaav9492.
11 X. Strakosas, H. Biesmans, T. Abrahamsson, K. Hellman, M. S. Ejneby and J. D. Mary, *Science*, 2023, **379**, 795–802.

12 N. Li, Y. Li, Z. Cheng, Y. Liu, Y. Dai, S. Kang, S. Li, N. Shan, S. Wai and A. Ziaji, *Science*, 2023, **381**, 686–693.
13 M. Hjort, A. H. Mousa, D. Bliman, M. A. Shameem, K. Hellman, A. S. Yadav, P. Ekström, F. Ek and R. Olsson, *Nat. Commun.*, 2023, **14**, 4453.
14 P. D. Howes, R. Chandrawati and M. M. Stevens, *Science*, 2014, **346**, 1247390.
15 A. H. Mousa, D. Bliman, L. Hiram Betancourt, K. Hellman, P. Ekstrom, M. Savvakis, X. Strakosas, G. Marko-Varga, M. Berggren, M. Hjort, F. Ek and R. Olsson, *Chem. Mater.*, 2022, **34**, 2752–2763.
16 K. Wang, G. Wang and M. Wang, *Macromol. Rapid Commun.*, 2015, **36**, 2162–2170.
17 S. Cheng, R. Zhao and D. S. Seferos, *Acc. Chem. Res.*, 2021, **54**, 4203–4214.
18 B. Carsten, F. He, H. J. Son, T. Xu and L. Yu, *Chem. Rev.*, 2011, **111**, 1493–1528.
19 H. Xiong, Q. Lin, Y. Lu, D. Zheng, Y. Li, S. Wang, W. Xie, C. Li, X. Zhang, Y. Lin, Z.-X. Wang, Q. Shi, T. J. Marks and H. Huang, *Nat. Mater.*, 2024, **23**, 695–702.
20 N. S. Gobalasingham and B. C. Thompson, *Prog. Polym. Sci.*, 2018, **83**, 135–201.
21 A. L. Mayhugh, P. Yadav and C. K. Luscombe, *J. Am. Chem. Soc.*, 2022, **144**, 6123–6135.
22 J.-R. Pouliot, F. Grenier, J. T. Blaskovits, S. Beaupré and M. Leclerc, *Chem. Rev.*, 2016, **116**, 14225–14274.
23 X. Zhang, Y. Shi, Y. Deng and Y. Geng, *Chin. J. Chem.*, 2023, **41**, 2908–2924.
24 S. J. Gilman, S. Saiev, J.-L. Brédas and J. R. Reynolds, *Macromolecules*, 2025, **58**, 4807–4818.
25 F. Grenier, K. Goudreau and M. Leclerc, *J. Am. Chem. Soc.*, 2017, **139**, 2816–2824.
26 Z.-R. Tan, Y.-Q. Xing, J.-Z. Cheng, G. Zhang, Z.-Q. Shen, Y.-J. Zhang, G. Liao, L. Chen and S.-Y. Liu, *Chem. Sci.*, 2022, **13**, 1725–1733.
27 F. Grenier, B. R. Aïch, Y.-Y. Lai, M. Guérette, A. B. Holmes, Y. Tao, W. W. H. Wong and M. Leclerc, *Chem. Mater.*, 2015, **27**, 2137–2143.
28 C. Wang, C. J. Mueller, E. Gann, A. C. Y. Liu, M. Thelakkat and C. R. McNeill, *J. Mater. Chem. A*, 2016, **4**, 3477–3486.
29 X.-L. Pei, Q. Yang, Y.-L. Sun, W. Wu, J.-Y. Yu and Y. He, *Chin. J. Polym. Sci.*, 2025, **43**, 718–729.
30 M. Lafrance, C. N. Rowley, T. K. Woo and K. Fagnou, *J. Am. Chem. Soc.*, 2006, **128**, 8754–8756.
31 D. Lapointe and K. Fagnou, *Chem. Lett.*, 2010, **39**, 1118–1126.
32 S. I. Gorelsky, D. Lapointe and K. Fagnou, *J. Org. Chem.*, 2011, **77**, 658–668.
33 B. Xiao, T. J. Gong, Z. J. Liu, J. H. Liu, D. F. Luo, J. Xu and L. Liu, *J. Am. Chem. Soc.*, 2011, **133**, 9250–9253.
34 D. Posevins, Y. Qiu and J. E. Backvall, *J. Am. Chem. Soc.*, 2018, **140**, 3210–3214.
35 P. X. Shen, L. Hu, Q. Shao, K. Hong and J. Q. Yu, *J. Am. Chem. Soc.*, 2018, **140**, 6545–6549.
36 Z. Wang, L. Hu, N. Chekshin, Z. Zhuang, S. Qian, J. Qiao and J.-Q. Yu, *Science*, 2021, **374**, 1281–1285.
37 Z. Zhuang and J.-Q. Yu, *J. Am. Chem. Soc.*, 2020, **142**, 12015–12019.
38 S. Z. Ali, B. G. Budaitis, D. F. A. Fontaine, A. L. Pace, J. A. Garwin and M. C. White, *Science*, 2022, **376**, 276–283.
39 J. Calleja, D. Pla, T. W. Gorman, V. Domingo, B. Haffemayer and M. J. Gaunt, *Nat. Chem.*, 2015, **7**, 1009–1016.
40 T. Korenaga, A. Ko, K. Uotani, Y. Tanaka and T. Sakai, *Angew. Chem., Int. Ed.*, 2011, **50**, 10703–10707.
41 Z.-H. Xie, G. Ye, H. Gong, P. Murugan, C. Lang, Y.-F. Dai, K. Yang and S.-Y. Liu, *Chem. Sci.*, 2025, **16**, 9998–10009.
42 B. Zhang, Y. Cai, L. He, N. Xu, Y. Yuan, J. Zhang, Y. Zhang and P. Wang, *Chem. Sci.*, 2024, **15**, 17103–17113.
43 H. Gong, J. Li, Z.-H. Xie, C. Lang and S.-Y. Liu, *Macromolecules*, 2024, **57**, 7208–7218.
44 C. A. Tolman, *Chem. Rev.*, 1977, **77**, 313–348.
45 S. Zhao, T. Gensch, B. Murray, Z. L. Niemeyer, M. S. Sigma and M. R. Biscoe, *Science*, 2018, **362**, 670–674.
46 S. I. Gorelsky, D. Lapointe and K. Fagnou, *J. Org. Chem.*, 2012, **77**, 658–668.
47 T. Lu and F. Chen, *Acta Chim. Sinica*, 2011, **69**, 2393–2406.
48 T. Lu and F. Chen, *J. Comput. Chem.*, 2012, **33**, 580–592.
49 Y. Q. Zhang, H. A. Lin, Q. C. Pan, S. H. Qian, S. H. Zhang, G. Qiu, S. C. Luo, H. H. Yu and B. Zhu, *ACS Appl. Mater. Interfaces*, 2020, **12**, 12362–12372.
50 W. Zhang, R. Jamal, R. Zhang, Z. Yu, Y. Yan, Y. Liu, Y. Ge and T. Abdiryim, *Phys. Chem. Chem. Phys.*, 2020, **22**, 3592–3603.
51 M. Hong, D. F. Perepichka and W. Fred, *Angew. Chem., Int. Ed.*, 2003, **42**, 589.
52 M. J. Frisch, G. W. Trucks, H. B. Schlegel, G. E. Scuseria, M. A. Robb, J. R. Cheeseman, G. Scalmani, V. Barone, B. Mennucci, G. A. Petersson, H. Nakatsuji, M. Caricato, X. Li, H. P. Hratchian, A. F. Izmaylov, J. Bloino, G. Zheng, J. L. Sonnenberg, M. Hada, M. Ehara, K. Toyota, R. Fukuda, J. Hasegawa, M. Ishida, T. Nakajima, Y. Honda, O. Kitao, H. Nakai, T. Vreven, J. A. Montgomery Jr, J. E. Peralta, F. Ogliaro, M. Bearpark, J. J. Heyd, E. Brothers, K. N. Kudin, V. N. Staroverov, T. Keith, R. Kobayashi, J. Normand, K. Raghavachari, A. Rendell, J. C. Burant, S. S. Iyengar, J. Tomasi, M. Cossi, N. Rega, J. M. Millam, M. Klene, J. E. Knox, J. B. Cross, V. Bakken, C. Adamo, J. Jaramillo, R. Gomperts, R. E. Stratmann, O. Yazyev, A. J. Austin, R. Cammi, C. Pomelli, J. W. Ochterski, R. L. Martin, K. Morokuma, V. G. Zakrzewski, G. A. Voth, P. Salvador, J. J. Dannenberg, S. Dapprich, A. D. Daniels, O. Farkas, J. B. Foresman, J. V. Ortiz, J. Cioslowski and D. J. Fox, *Gaussian 09, Revision E.01*, Gaussian, Inc., Wallingford CT, 2013.
53 Y. Zhao and D. G. Truhlar, *J. Chem. Phys.*, 2006, **125**, 194101.
54 I. A. Guzei and M. Wendt, *Dalton Trans.*, 2006, **33**, 3991–3999.
55 E. D. Glendening, A. E. Reed, J. E. Carpenter, and F. Weinhold, *NBO Version 3.1*.